PAPER

Regulatory effects of gradient microtopographies on synapse formation and neurite growth in hippocampal neurons

To cite this article: Ryan McNaughton et al 2022 J. Micromech. Microeng. 32 075005

View the article online for updates and enhancements.

You may also like

- Effects of metal fluoride/sulfide microparticles generated by consecutive high-pulse-power breakdowns on the insulating performance in compressed SF₆ Wenlong Yan, Zhenxing Wang, Wei Shang et al.
- Collagen hydrogels with controllable combined cues of elasticity and topography to regulate cellular processes
 Tomoko G Oyama, Kotaro Oyama, Atsushi Kimura et al.
- Three-dimensional CaP/gelatin lattice scaffolds with integrated osteoinductive surface topographies for bone tissue engineering Danish Nadeem, Carol-Anne Smith,

Danish Nadeem, Carol-Anne Smith Matthew J Dalby et al.

J. Micromech. Microeng. 32 (2022) 075005 (12pp)

https://doi.org/10.1088/1361-6439/ac73d7

Regulatory effects of gradient microtopographies on synapse formation and neurite growth in hippocampal neurons

Ryan McNaughton^{1,5}, Yuda Huo^{2,5}, Guicai Li^{1,5}, Anais Di Via Ioschpe², Lei Yan¹, Heng-Ye Man^{2,4,*} and Xin Zhang^{1,3,*}

E-mail: hman@bu.edu and xinz@bu.edu

Received 7 February 2022, revised 4 May 2022 Accepted for publication 26 May 2022 Published 10 June 2022



Abstract

Among approaches aiming toward functional nervous system restoration, those implementing microfabrication techniques allow the manufacture of platforms with distinct geometry where neurons can develop and be guided to form patterned connections in vitro. The interplay between neuronal development and the microenvironment, shaped by the physical limitations, remains largely unknown. Therefore, it is crucial to have an efficient way to quantify neuronal morphological changes induced by physical or contact guidance of the microenvironment. In this study, we first devise and assess a method to prepare anisotropic, gradient poly(dimethylsiloxane) micro-ridge/groove arrays featuring variable local pattern width. We then demonstrate the ability of this single substrate to simultaneously profile the morphological and synaptic connectivity changes of primary cultured hippocampal neurons reacting to variable physical conditons, throughout neurodevelopment, in vitro. The gradient microtopography enhanced adhesion within microgrooves, increasing soma density with decreasing pattern width. Decreasing pattern width also reduced dendritic arborization and increased preferential axon growth. Finally, decreasing pattern geometry inhibited presynaptic puncta architecture. Collectively, a method to examine structural development and connectivity in response to physical stimuli is established, and potentially provides insight into microfabricated geometries which promote neural regeneration and repair.

1

Supplementary material for this article is available online

Keywords: gradient microtopography, primary cultured hippocampal neuron, microenvironment interaction, neurite extension, synaptic connectivity

(Some figures may appear in colour only in the online journal)

1361-6439/22/075005+12\$33.00 Printed in the UK

© 2022 IOP Publishing Ltd

¹ Department of Mechanical Engineering, Boston University, Boston, MA, 02215, United States of America

² Department of Biology, Boston University, Boston, MA, 02215, United States of America

³ Photonics Center, Boston University, Boston, MA, 02215, United States of America

⁴ Center for Systems Neuroscience, Boston University, Boston, MA, 02215, United States of America

⁵ Contributed equally.

Author to whom any correspondence should be addressed.

1. Introduction

To gain insight into neuronal regeneration and repair processes at a cellular level, simpler culture platforms are required to reduce the cellular network complexity while maintaining similarity to the physiological condition. Methods for enhancing neural circuit formation have been investigated in vitro [1], from micromachining [2-5] to self-assembly [6, 7]. Regeneration models of peripheral axonal injury have been studied via microfluidic devices [8, 9], and implantable polymeric scaffolds [10–12]; however, there remains a lack of optimal approaches [13] to restore central nervous system function. Typical regenerative tools emphasize electrical [14] or chemical [15] stimulation on culture plates or within microfluidic platforms [16, 17], but do not reveal the impact of physical cues. Neurons experience higly variable density and molecular cues in the native extracellular matrix (ECM) [18], so a systematic methodology to evaluate neuronal network formation is needed.

In vitro platforms manipulate the cell-microenvironment interaction and provide physical contact cues to influence neuronal development [19, 20]. Micro/nano-gratings on soft materials enhance the differentiation of neural progenitor cells [21]. Pillar arrays or grooves manipulate the soma distribution [22], the neurite orientation and outgrowth [23], and the synapse formation [24, 25]. Soft [26] and patterned semiconductor [27] micro/nanotopographies demonstrated an ability to induce differentiation, alignment, and neurite extension. The manufacturing simplicity of these topographies allows for highly controlled studies of neuronal cell behavior with dramatically altered mechanical stimuli via physical cues. These topographic structures are singly fabricated, necessitating a multitude of substrates, increasing the experimental runtime and risk of contamination, and decreasing systematic observation of the topographical effects.

Progress has been made in the development of gradient biomaterials with spatially variable chemical (immobilized molecules) or physical (topographic structures) properties, mimicking the *in vivo* microenvironment [23, 28, 29]. Micropatterns of octacalcium enhanced controllability of cell immobilization [30]. Gradient density, linear microarrays modulate cancerous and normal cell migration and alignment [31, 32]. For neuronal cells, gradient micro/nanopillars regulated differentiation, neurite extension, and enhanced guidance [33, 34]. Printing and microfluidics have also been implemented to improve axonal guidance and stem cell culture systems [35–37]. While these results are promising, there exists a necessity for devices capable of comprehensively screening neurite and synapse formation, as few studies on the influence of physical contact cues from gradient ridge/groove microtopographies on hippocampal neuron morphogenesis and maturation have been reported [29, 38].

Herein, we demonstrate a rapid technique to prepare gradient, anisotropic micro-ridge/groove arrays with variable local pattern width for culturing primary hippocampal neurons. Neurite outgrowth behavior, such as axon elongation and dendritic branching, and formation of synapses were quantitatively investigated using an immunochemistry method. It was

anticipated this study may demonstrate the ability of a gradient microtopography (GM) to provide a more comprehensive understanding of the neuron-microtopography interaction.

2. Materials and methods

2.1. Design of the GM

The gradient micro-ridge/groove array was designed using AutoCAD Design Software (Autodesk, San Rafael, CA, USA). Three distinct GMs were designed, consisting of linear microchannel structures with varying widths and depths. The channel depths were constant for a given design, denoted GM 3, 6 and 10, corresponding to 3 μ m, 6 μ m, and 10 μ m depths, respectively. The microchannel width varied for each design in the following fashion: 5 μ m, 20 μ m, 40 μ m, and 80 μ m [39] (figure 1).

2.2. Fabrication of the GM

Poly(dimethylsiloxane) (PDMS) samples were fabricated using soft lithography to transfer the GM from silicon molds (figure 2). Molds were fabricated from 4 inch, P-doped (<100>), silicon wafers (University Wafer, South Boston, MA, USA) with photolithographic techniques and etched with deep reactive ion etching (DRIE; High Rate HRMASE, STS, Newport, UK). The base and curing agent from a Sylgard 184 Silicone Elastomer Kit (Thermo Fisher Scientific, Waltham, MA, USA) were mixed in a 10:1 ratio, degassed at room temperature, poured onto the silicon master molds, and cured at 120 °C for 40 min in a vacuum oven. Thereafter, the samples were peeled from the molds resulting in substrates with surface topography spanning a $10 \times 10 \text{ mm}^2$ area. Samples were treated with oxygen plasma (M4L, PVA TePla America, Corona, CA, USA) at 300 W and 150 seem for 5 min to increase hydrophilicity. The surface was coated with poly-Dlysine/laminin (Sigma-Aldrich, St. Louis, MO, USA) under vacuum until dry, sterilized in 70% ethanol, and incubated in 15 mM poly-L-lysine (Sigma-Aldrich, St. Louis, MO, USA) solution at room temperature for 1 week. Finally, PDMS substrates were washed with phosphate buffered saline (PBS) to remove toxin residues prior to cell seeding.

2.3. GM characterization

2.3.1. Surface geometry. The surface geometry of the prepared PDMS GM was measured with a Nikon Eclipse LV150 optical microscope. Sample preparation began by cleaning the PDMS gradients using 100% ethanol, and DI water. Cross-sections (500 μ m thick) were cut at the midpoint of each geometric region, mounted on a microscope stage, and observed using 50× magnification. The dimensions of each cross-section were measured by an embedded NIS-Elements D software package. Three images per cross-section were captured and 15 width and depth measurements were recorded (table 1, figure S1 (available online at stacks.iop.org/JMM/32/075005/mmedia)). The GM was also observed under a scanning electron microscope (Carl Zeiss

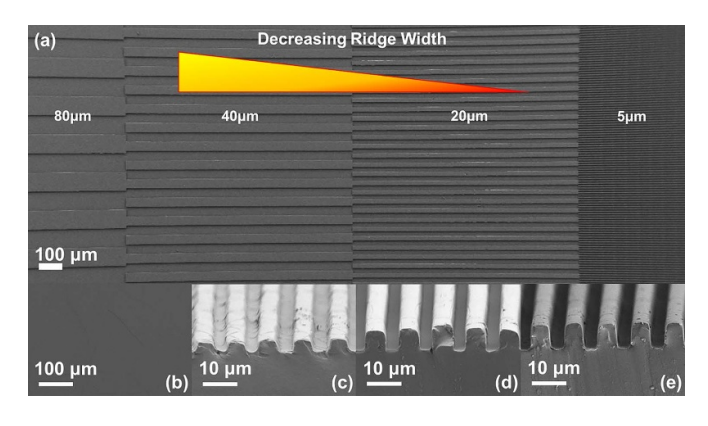


Figure 1. Scanning electron microscope images of PDMS substrate demonstrating reproducibility and continuity of the GM. Results of the fabrication protocol depicting (a) one half of the continuous gradient along the GM, (b) a flat control (top view), and (c)–(e) a transverse view of multiple GMs with depths of 3 μ m, 6 μ m, and 10 μ m (constant 5 μ m width). GM = gradient microtopography.

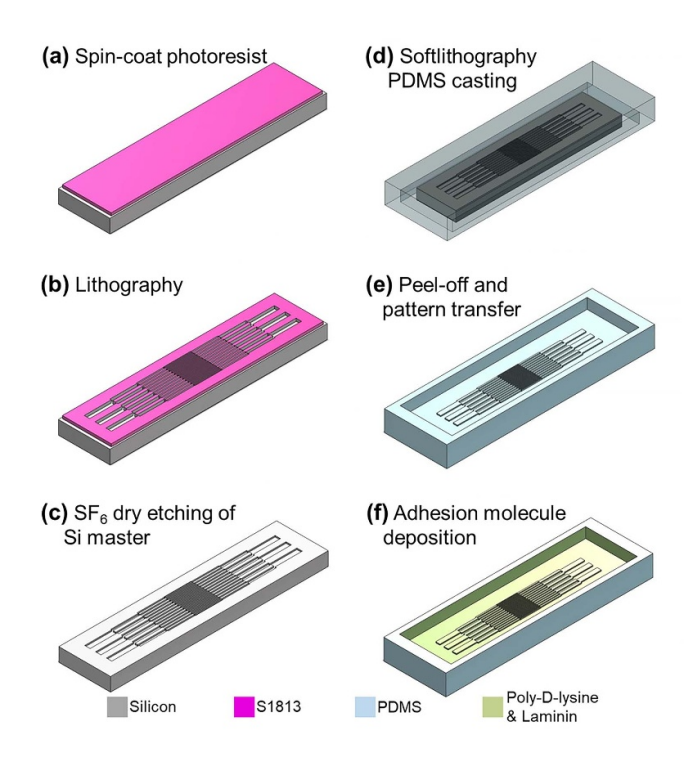


Figure 2. Fabrication protocol. The GM substrate was fabricated by (a) spin-coating a silicon wafer with S1813 positive tone photoresist, (b) photolithographically patterning the resist, (c) deep reactive ion etching the wafer anisotropically to 3 μ m, 6 μ m, or 10 μ m and stripping the photoresist to create a master mold, (d) coating with PDMS prepolymer, (e) thermally curing the PDMS for pattern transfer, and (f) adsorbing poly-D-lysine and laminin to the surface under vacuum. GM = gradient microtopography. PDMS = poly(dimethylsiloxane).

Microscopy, Peabody, MA, USA) to check for topography stability. The PDMS substrate was sputter coated with a 5 nm layer of gold nanoparticles (Cressington 108, Ted Pella, Redding, CA, USA). Observation was performed under a 1×10^{-6} Torr system vacuum.

Table 1. Summary of GM dimensions. All data are presented as mean \pm standard deviation, with units in μ m. GM = gradient microtopography.

	GM3	GM6	GM10
Substrate depth	3.52 ± 0.45	7.23 ± 0.38	9.30 ± 0.36
5 μ m section	5.12 ± 0.34	5.25 ± 0.35	4.71 ± 0.29
$20 \ \mu m$ section	20.01 ± 0.56	19.86 ± 0.28	19.43 ± 0.32
$40 \ \mu m$ section	39.56 ± 0.68	38.97 ± 0.39	38.80 ± 0.33
$80 \ \mu m$ section	77.90 ± 1.15	77.45 ± 0.36	77.90 ± 1.15

2.3.2. Substrate wettability assessment. The GM wettability before and after plasma treatment was measured via static water contact angle (WCA) measurement. GM substrates were placed on a custom stage and aligned with a glass magnifying lens (figure S2). A digital camera (EOS 400D, Canon, Melville, NY, USA) was then used to photograph the contour of the droplet above the patterned area. WCA measurements before and after oxygen plasma treatment (300 W, 150 sccm, 5 min) were recorded using ImageJ (NIH, Rockville, MD, USA). Three substrates of each depth were fabricated to record the relative change.

2.3.3. Fourier transform infrared spectroscopy (FTIR). FTIR spectroscopy (Nexus 670, Nicolet FTIR, Thermo Fisher Scientific, Waltham, MA, USA) evaluated the surface components present in the GM samples at various stages of the fabrication process. PDMS with and without surface enhancement via poly-D-lysine/laminin coating had their chemical components identified. Differences in the respective infrared absorption spectra (400–4500 cm⁻¹) were compared to identify the presence of chemical residues found in laminin for promoting neuronal adhesion. Samples were placed face down on the measurement stage while the spectra were recorded (figure S3).

2.4. Isolation and culture of hippocampal neurons

Primary cultured hippocampal neurons were prepared from embryonic day 18 (E18) rats. E18 pregnant Sprague-Dawley rats were purchased from Charles River Laboratories Inc. Briefly, embryonic hippocampi were dissected and digested with papain at 37 °C for 20 min. After trituration, dissociated hippocampal neurons were collected by centrifuge at 2100 rpm for 3 min, re-suspended in plating medium, and seeded evenly onto the PDMS GM samples at a density of 5×10^4 cells. Excess cells were plated into the surrounding 6 cm petri dish at a density of 6×10^5 cells to support overall viability but are not considered in the analyses described herein. The GM and flat controls were first coated with poly-D-lysine/laminin and then soaked in poly-L-lysine for 7 days, before being fixed to the bottom of the culture dish for cell plating. Neurons were maintained in Neurobasal medium (Gibco) supplemented with 2% Neurocult SM1 Neuronal Supplement (StemCell Technologies), 1% horse serum (Atlanta Biologicals), 1% penicillin/streptomycin (Corning), and L-glutamine

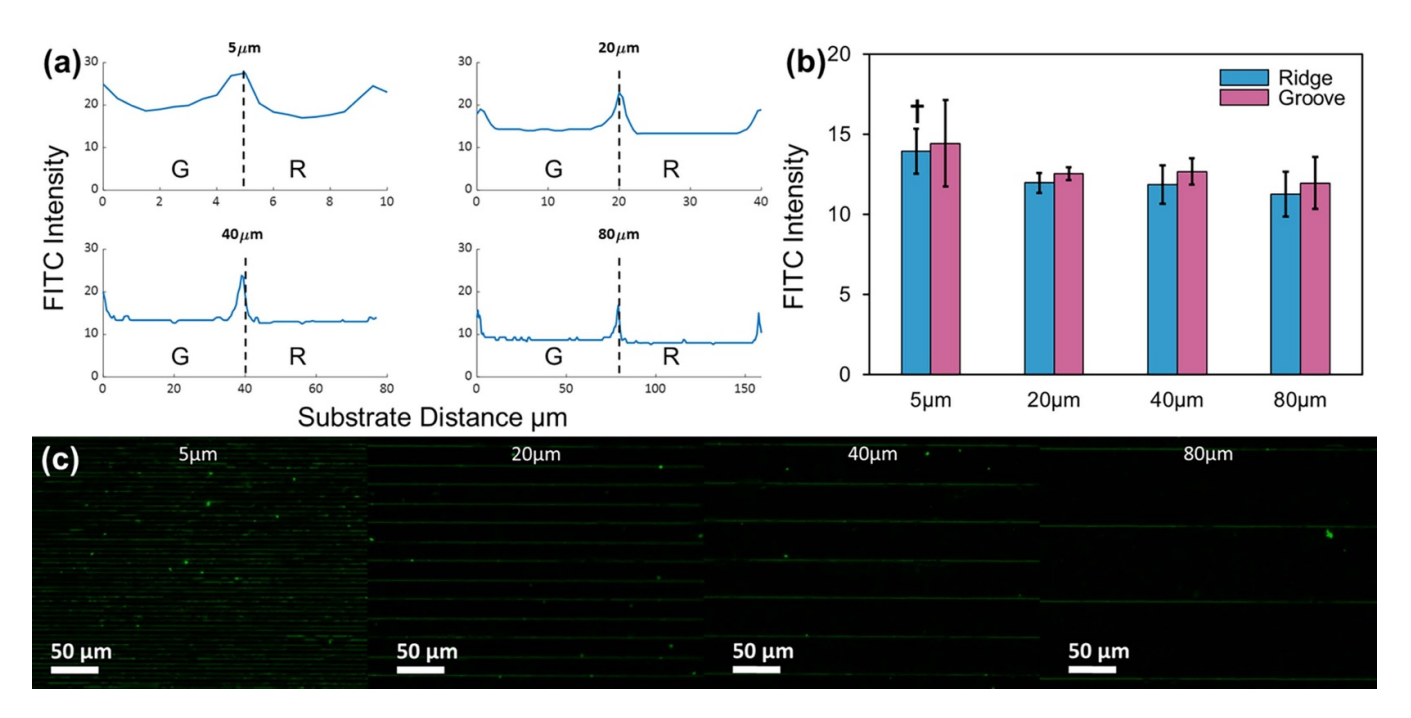


Figure 3. Surface coating of adhesion proteins assessed via FTIR spectroscopy (figure S3(a)), and line plots (a) and (b) cross-sectional average of fluorescent intensity measurements. (c) Representative images of each pattern width and constant, 3 μ m depth. Fluorescence of FITC-labelled poly-L-lysine coating shown in green. Minimal, nonsignificant increases in fluorescence are shown. †, P < 0.05. FTIR = Fourier transform infrared spectroscopy. FITC = fluorescein isothiocyanate.

(Corning). 5'-fluoro-2'-deoxyuridine (10 μ M, Sigma-Aldrich, St. Louis, MO, USA) was applied to neuron media eight days post cell plating to suppress glial growth until experimentation. All cells were maintained in a humidified incubator at 37 °C in an atmosphere containing 5% CO₂.

2.5. Immunostaining and image collection

To access structural properties, hippocampal neurons on the GMs were washed with PBS, fixed with 4% paraformaldehyde plus 4% sucrose for 10 min, and permeabilized with 0.3% Triton X-100 in PBS for 10 min at room temperature. After 1 h blocking with 10% goat serum in PBS, cells were incubated with antibodies against microtubule associated protein 2 (MAP2; rabbit, 1:1000) and Tau-1 (mouse, 1:1000) for 1 h at room temperature. They were then washed with PBS twice and incubated with fluorophore-conjugated secondary antibodies (Alexa Fluor 405 blue anti-rabbit, 1:500 and Alexa Fluor 555 red anti-mouse, 1:500) for 1 h at room temperature. To access network forming capabilities, cells were incubated post-blocking with Synapsin 1 (rabbit, 1:1000) overnight at 4 °C, washed with PBS twice, and incubated with fluorophore-conjugated secondary antibody (Alexa Fluor 555 red anti-rabbit, 1:500) for 1 h at room temperature. GMs were then mounted on glass microscopy slides with an antifade mountant (Prolong Gold Antifade Mountant, Thermo Fisher Scientific, Waltham, MA, USA). Hippocampal neurons fixed to the GM were imaged with a Carl Zeiss inverted fluorescent microscope by $40 \times$ air and $63 \times$ oil-immersion objectives. Images were collected by AxioVision 4.5 software. First, a phase snap was taken. The exposure time was set automatically by the software and adjusted manually such that the signals fell within the full dynamic range. To compare neurons across the GM, the exposure time remained constant for each fluorophore-labeled protein.

A solution of fluorescein isothiocyanate (FITC)-labeled poly-L-lysine at 0.1 mg ml^{-1} in PBS (Sigma-Aldrich, St. Louis, MO, USA; figure 3) was prepared to validate coating uniformity following the 7 day incubation protocol. GMs incubated in this solution were not plated with neurons. Following incubation, GMs were mounted to glass slides with an antifade mountant and observed under the $40\times$ air objective. The distribution of fluorescence along the GM was measured for surface homogeneity.

2.6. Morphological index analysis

2.6.1. Preferential neuronal residence measurement. The residential preference of hippocampal neuron somas was assessed by comparing soma number in each geometric area. Somas were selected as an identifier of location to sequester neurites crossing multiple ridge/groove complexes. The total number of somas located inside a groove or on top of a ridge was converted into an area density measurement, defined with ImageJ's area selection tool. This calculation was conducted for each geometric region along the surface the three microtopography conditions (GM3, GM6, and GM10), evaluating adhesion preference as a function of width and depth. To eliminate adhesion bias from surface coating errors, the relative fluorescent intensity of FITC-PLL across each GM was quantified. For every experiment, measurements of 50 somas, were collected in each topographical region.

2.6.2. Preferential axonal outgrowth assessment. In addition to soma preference, axon growth in the presence of physical cues was examined by analyzing the outgrowth of neurites. In particular, the relative fluorescent signal intensities of axonal segments in the groove and on the ridge were measured. Axons were stained with anti-Tau-1 primary antibody and fluorescently labeled (Alexa Fluor 555) secondary antibody. Axons were isolated from the other neurites by overlaying dendritic processes stained with anti-MAP2 primary antibody and removing those overlapping. The fluorescent signal intensity was measured along the surface of adjacent ridges and grooves, parallel to the width. The signal intensity was measured every 0.5 μ m. This was conducted on ten ridge/groove cross-sections for each GM region resulting in a minimum of 100 measurements. The average fluorescence signal intensity along the line in each ridge/groove was calculated.

2.6.3. Dendritic arborization assessment. The area spanned by dendritic arborizations was measured. A polygon was drawn by linking the dendrite tips of the arborization and calculating the enclosed microscale area with ImageJ. Dendritic segments were identified by staining neuron specific MAP2 protein with antibody conjugated with Alexa Fluor 405 fluorochrome. Each experiment considered 50 arborizations. Differentiated axons were excluded from measurement to isolate dendritic neurites and their associated arborization. Through this analysis, the network-forming potential of neurons in each GM condition was quantified.

2.7. Synaptic connectivity assessment

Synaptic connectivity was quantified by assessing the relative density and fluorescent intensity of the presynaptic marker protein Synapsin 1. Images were adjusted to a fluorescent threshold which passed approximately 3% of the total expressed protein intensity. Furthermore, only thresholded objects with area between 0.08 and 2.56 μ m² were considered presynaptic puncta. Fifty distinct area measurements were obtained for each geometric region. Within an individual groove or ridge area, the total number of synapses was converted to synaptic puncta density. Additionally, the Synapsin 1 intensity for each punctum was averaged, providing a relative fluorescence measurement within a given topography. Area measurements were exclusively taken around axon-to-dendrite synapses, eliminating potential biasing from synapses formed with the soma.

2.8. Statistical analysis

All measurements were conducted with ImageJ version 1.43 software. Twelve biologically independent hippocampal neuron cultures were conducted, with four cultures carried out until DIV 4, DIV 7, and DIV 14, respectively. For each of the four cultures, three substrates with identical topography (flat controls, GM3, GM6, or GM10) were fixed to the bottom of a culture dish and plated with hippocampal neurons. For morphological and synaptic connectivity measurements,

data points were grouped based on the topographical geometry. Groups were compared using a two-sample unequal variance two-tailed t-test, with P < 0.05 indicating statistical significance.

3. Results

3.1. GM characterization

The dimensional continuity of each geometric region was assessed prior to plating cells. The anisotropic GM is shown in figure 1, with structure width ranging from 80 μ m wide to 5 μ m wide ridges and grooves. The reproducibility of 5 μ m wide regions required special attention, ensuring no errors occurred during polymeric pattern transfer. Figures 1(c)–(e) shows representative cross-sections of this region, with GM depths of 3 μ m, 6 μ m, and 10 μ m, respectively. These images show high reproducibility, including regions with the highest aspect ratio where capillary forces can dominate and distort the geometry (figure 1(e)). The average widths and depths of each region on the topography are shown in table 1 and were observed to be significantly different (figures S1(b) and (c)).

3.2. Analysis of preferential neuronal residence

Neuronal adhesion after plating is a prerequisite for future developmental stages such as neurite outgrowth and formation of synaptic connections. To assess the effects of variable geometries on cell adhesion and viability, we examined the soma residence preference. To this end, primary hippocampal neurons plated onto the surface of the GM were fixed at DIV 4, DIV 7 and DIV 14, respectively. The soma was visualized by the overlap of the dendritic marker protein, MAP2, and axon marker protein, Tau-1.

At DIV 4, neuron density increased per unit area compared to flat topography controls. This remained true for geometric widths across the microtopography, regardless of their depth. Furthermore, decreasing pattern width for each GM depth significantly increased neuron density, with enhancement ranging from 18.4% (80 μ m ridges) to a maximum of 329.9% for 20 μ m grooves, over flat controls. Neurons cultured on GM3 (figure 4(a)) and GM6 (figure S6(a)) induced preferential adhesion within the microchannels (20 μ m, 40 μ m, and 80 μ m); however, GM6 reduced preferential adhesion within 20 μ m microchannels relative to GM3 and GM10. When pattern width decreased to 5 μ m, which is below the average soma diameter (15–25 μ m), preferential adhesion ocurred atop the ridge. Restricting the neurons capability to adhere within the microchannel, resulted in elevated enhancement of 616.2% over controls (figure 4(a)). For GM3, microchannels of large patterns ($\geq 20 \mu m$) enhanced neuron density by $98.7 \pm 20.3\%$, on average, compared to density on top of the ridge. On the smaller 5 μ m topography, 64.8% fewer cells adhered within the microchannel compared to ridge, resulting in a 25.6 \pm 14.5% reduction of soma density relative to large grooves. Neurons adhered within the 5 μ m microchannel were observed to have elongated soma morphology, although this finding was not quantified (figure 4(c)).

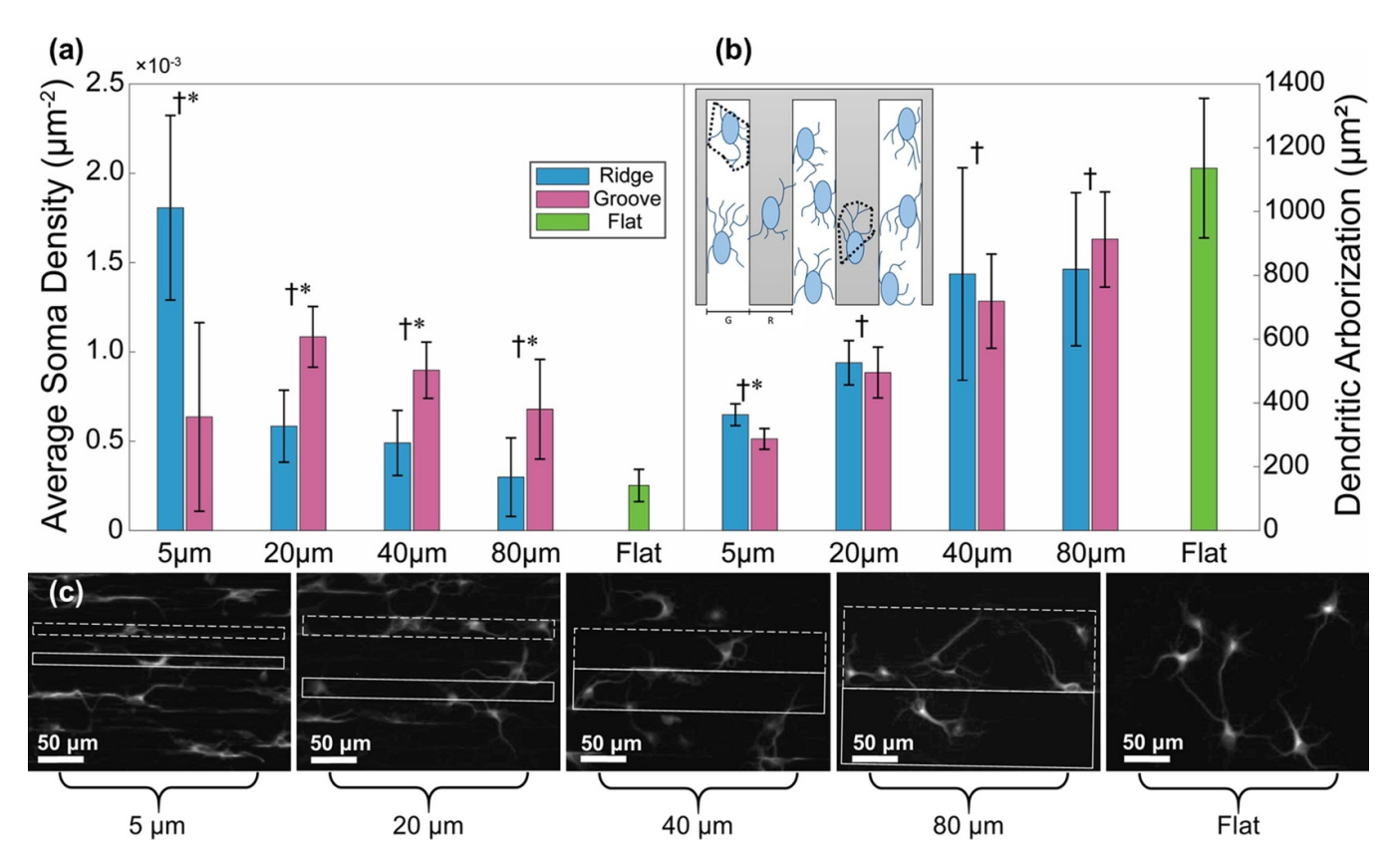


Figure 4. Morphological analysis of the MAP2 channel acquired on GM3 at DIV 4. (a) Cell density and (b) dendritic tree (arborization) expansion are inversely proportional in the presence of linear ridge (solid)/groove (dashed) microtopography. (c) Representative images of individual cells in each region of GM3. Inset: example arborization area calculation. * , P < 0.05 groove vs ridge; \dagger , P < 0.05 vs flat. MAP2 = microtubule associated protein 2. GM = gradient microtopography. DIV = days *in vitro*.

3.3. Analysis of preferential axonal outgrowth and dendritic arborization

Following neuron adhesion, neurites, including dendrites and axons, begin to extend from the soma. Dendritic arborization was visualized by immunofluorescent labeling of dendritic specific marker MAP2 at DIV 4. Combined with image processing tools, the area covered by the corresponding dendrites was quantified in the presence of physical topography. In comparison to flat controls, substrate microtopography hindered the expansion of neurites. Dendrite labeling at DIV 4 showed increasingly aligned and constrained dendritic arborizations calculated according to figure 4(b) (inset), consistent throughout each of the geographic regions. In 40 and 80 µm wide environments, dendritic expansion exhibited a $23.7 \pm 4.1\%$ reduction in coverage area. Across the GM the neurons adhered within microchannels experienced a significant, linear reduction ($R^2 = 0.993$) in dendritic arborization area: 5 μ m, 287.3 \pm 32.6 μ m²; 20 μ m, 495.3 \pm 79.7 μ m²; 40 μ m, 718.9 \pm 147.6 μ m²; 80 μ m, 913.5 \pm 148.0 μ m². This regression was also true of neurons resting on top of neighboring ridges ($R^2 = 0.915$). In general, as the density of the cells increased, the corresponding dendritic arborization area decreased. While microchannels enhanced adhesion and cell viability (figure 4(a)), they did not exhibit a significant arborization area reduction relative to neurons cultured on ridges of the same dimension. One exception occurred on 5 μ m wide patterns from GM3, which induced significant (20.9%) reductions in dendritic arborization area within microchannels (figure 4(b)).

During in vitro development, axonal polarization of hippocampal neurons occurs within 48 h post plating. To study the effects of the GM on axons following differentiation, we fixed neurons at DIV 4 and labeled the corresponding axons using antibodies against axonal specific marker Tau-1 (figures 5(a)-(e)). Relative fluorescence in each pattern was measured (figure 5(f)), with representative curves for the fluorescence across a single ridge/groove complex shown in figure 5(h). The fluorescence was not evenly distributed, with enhanced signal intensity observed centrally in both grooves and ridges. Tau-1 signal intensity migrates toward the periphery with increasing topography width. The average fluorescent intensity in each of the GM regions generally increased as the pattern width decreased, while the microchannels consistently exhibited a higher presence of Tau-1 (figure 5(g)). As the width of the topography on GM3 decreased, the Tau-1 signal intensity within the microchannels increased by $32.1 \pm 7.0\%$. The fluorescence in the 40 μ m region was not significantly different, however, all other dimensions demonstrated an average enhancement of 42.4 \pm 5.8%. Fluorescent signal intensity of Tau-1 in axons grown on GM6 and GM10 was only different from those on GM3 for 5 μ m topographies (figure S7). On average, 5 μ m topographies induced fluorescent intensity

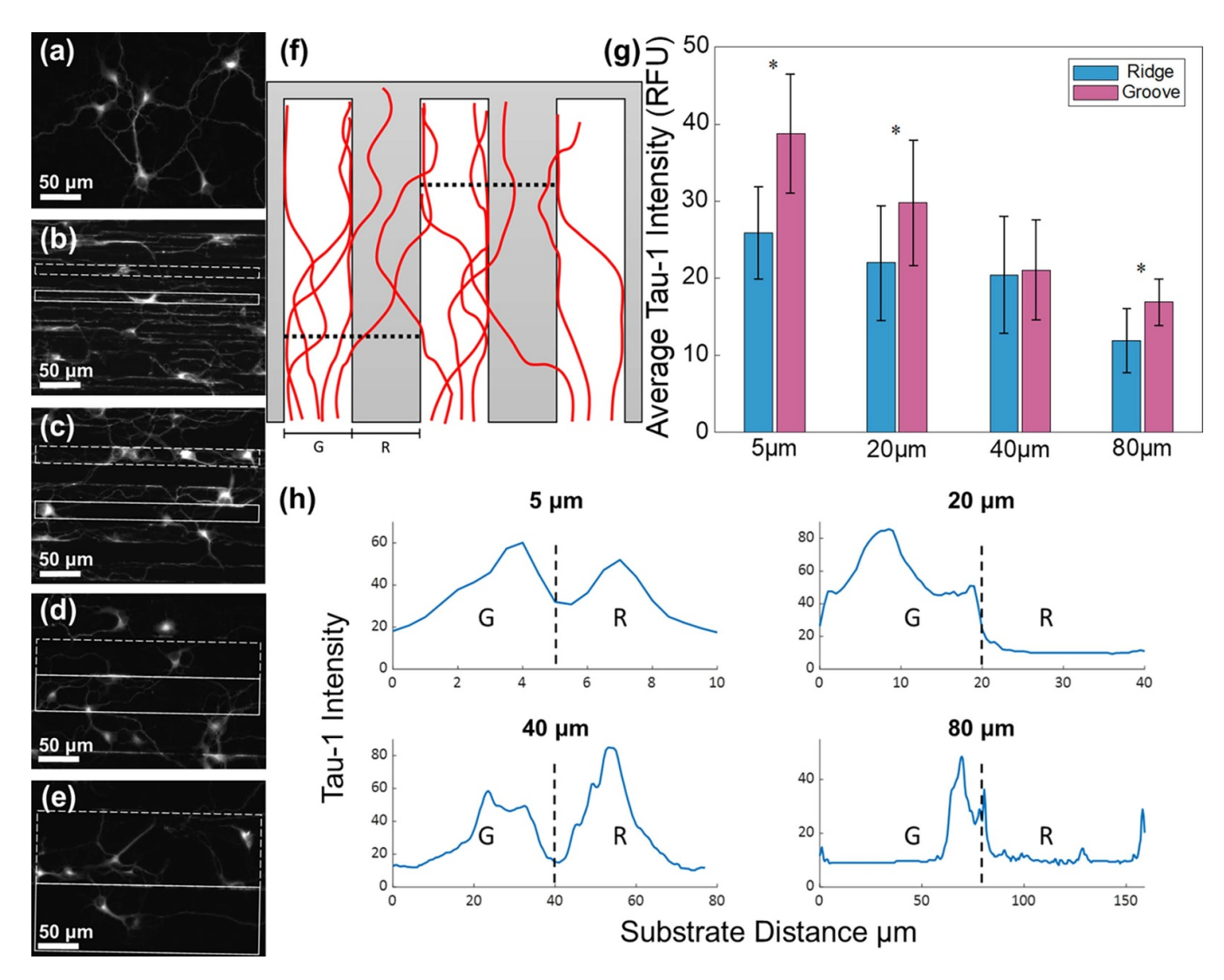


Figure 5. Axonal maturation under exposure to various microtopographies with constant 3 μ m depth. Neurons were cultured until DIV 4. Representative images of individual cells on (a) flat controls, and GM3: (b) 5 μ m wide, (c) 20 μ m, (d) 40 μ m, (e) 80 μ m topographies. (f) Example axon growth preference calculation. Black dotted lines plot Tau-1 intensity with the average along the cross-section shown in (g). (h) Line plots of the protein expression within each topographical area for a single ridge/groove complex. Most of the protein expression is localized to the center of the pattern and extends toward the periphery with increasing pattern width. *, P < 0.05 groove versus ridge. DIV = days *in vitro*. GM = gradient microtopography.

on GM6 that was $94.4 \pm 5.5\%$ higher than GM3 and GM10 for axons growing on top of ridges, and $36.3 \pm 6.9\%$ within the microchannels. Flat controls were not considered in this experiment, due to spatially random axon growth.

3.4. Analysis of presynaptic biomarkers on GM

To assess connectivity, we used the presynaptic marker protein Synapsin 1 to indicate the presynaptic site. The relative puncta per unit area of microtopography, and average punctum protein signal intensity were quantified through immunofluorescent staining at DIV 14 and analyzed with ImageJ. The Synapsin 1 stained puncta density was enhanced on narrow, 5 μ m regions of GM3; however, topographies generally demonstrated no increase in synaptic density relative to flat controls, contradicting expected increases due to the previously discussed increase in cell density (figures 4(a) and 6(a)). GM3

topographies on average showed a $24.8 \pm 17.1\%$ increase in synapses formed within microchannels versus on top the pattern, while the deeper topography GM10 induced a sparser network, with $7.14 \pm 8.6\%$ fewer synapses per unit area in the microchannels (figure S8(a)).

Synapsin 1 fluorescent intensity for neurons from GM3 decreased on 40 μ m and 80 μ m microtopographies relative to flat controls, while 5 μ m and 20 μ m topographies only demonstrated significant decreases for synapses located above the pattern (figure 6(b)). GM10 also exhibited a significant decrease in Synapsin 1 signal intensity for synapses formed on neurites extending along the tops of ridges (figure S8(b)). Examining each individual pattern width revealed a significant increase in Synapsin 1 signal intensity for synapses formed within microchannels versus on top of the ridges, $46.5 \pm 14.4\%$ and $52.4 \pm 17.6\%$, for GM3 and GM10, respectively. GM3 topographies did not enhance Synapsin 1 signal

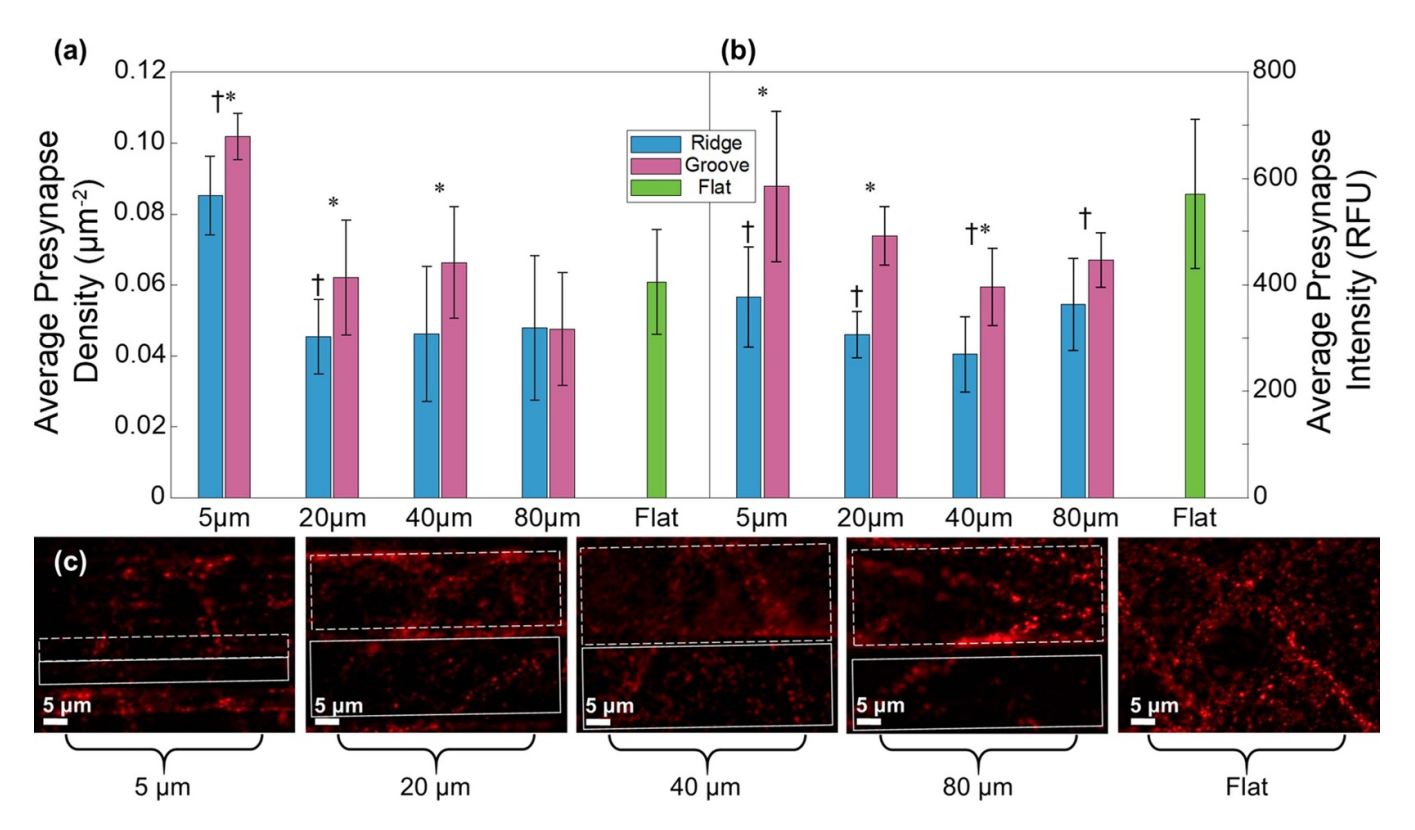


Figure 6. Quantification of synapses immunostained with anti-Synapsin 1 at DIV 14. (a) Presynapse puncta density and (b) protein expression increases within the smallest pattern width; however, topography generally inhibits presynapse architecture. (c) Representative images showing the change in presynaptic density and Synapsin 1 expression across the microtopographical substrate. Fluorescence of Synapsin-1 shown in red. Ridges are shown in solid boxes and grooves in dashed. *, P < 0.05 groove versus ridge; †, P < 0.05 versus flat. DIV = days *in vitro*.

intensity relative to flat controls; however, a general increasing trend was induced as the topography width decreased from 80 μ m to 5 μ m. Representative images of neurons cultured on flat controls and GM3 topographies reflect these findings. Clear localization and enhanced fluorescence of Synapsin 1 was observed within the grooves (figure 6(c)).

4. Discussion

It has been previously reported that the use of microtopographies for contact guidance of neuronal cells influenced the extension [11, 40] and alignment of neurites [29], the orientation of the soma [38, 41], initial polarization [33], and differentiation of neural progenitors [21, 27, 42]. While informative for understanding the influence of surface topographies on neural tissue, there is a lack of methodologies and substrates for systematic and comprehensive assessment of physical, topographic cues using variable geometry. As such, it was the goal of this study to create and implement a method of assessing neuronal response to microtopographical stimuli. A GM, comprised of adjacent linear, anisotropic microtopographies with variable geometry, was fabricated along a single substrate through a photolithographic and PDMS micromolding technique (figure 2) and surface modified (figures 3 and S3) with adhesion proteins [39]. Topography widths were varied from 5 μ m to 80 μ m and depths from 3 μ m to 10 μ m to facilitate a variety of cell interactions with the microenvironment. This fabrication method allowed morphological and synaptic screening of hippocampal neurons in a variety of environments with a fourfold decrease in the fabrication time relative to singly fabricated substrates. Ultimately, the GMs will lead to a better understanding of the neuronmicroenvironment interaction as well as more rapid development of microtopographical culture substrates.

Following genesis in the CNS, neurons migrate to and mature in their phenotypically defined destinations through contact with radial glia and the local microenvironment. Membranous sheets of lamellipodia and filopodia probe the local environment for attractive and repulsive cues, which dictate guidance [43]. Hippocampal neurons translate through the hippocampus in this same manner, attaching lead processes to radial glial fibers and climbing to their desired location [44]. Studying this contact guidance with topographies have commonly been used for neurite elongation, which is imperative for nerve repair [11, 45]. Implementation of a GM is more advantageous for a complete understanding of how contact guidance influences neuron morphology and network formation through interaction with the ECM [29, 41]. Through a simultaneous screening of neurons in each topographical region, trends in the morphological outcomes and network forming potential can be deduced. First, at these length scales, the topography acts as a physical barrier confining neuronal adhesion and neurite outgrowth. Second, topography generally hinders the ability of neurons to form active networks.

Decreasing ridge/groove topography width demonstrated increased cellular adhesion and viability. Feature density has previously been demonstrated to cause cell migration [28, 31, 32, 46]; however, this large-scale movement is not common for the neuron population, which readily adhere after identifying a viable location. In this work, we observed elevated soma density as the width of the GM decreased (figure 4(a)). Furthermore, somas adhered more readily within the microgrooves along the GM [39]. Cortical neurons have shown similar preference for microgrooves at geometries approximately equal to or a few times larger than the soma diameter [47]. In the case of 5 μ m wide regions some soma even elongated to adequately fit into the microgroove, although this is not common (figure 4(c)). Immunostaining of a blank GM confirmed no adhesion molecule bias was influencing the experiment. The groove and ridge surfaces expressed equivalent poly-L-lysine fluorescence (figures 3(b) and (c)); however, the presence of three coated surfaces (groove and two side walls) was likely a more favorable environment for cell viability. Reducing the topography width therefore increases the favorable surface area for adhesion, allowing more cells to survive throughout culture. To confirm the findings of our study time lapse recording of the neurons through DIV 1 is required and will allow observation of the migration and adhesion processes.

Axonal pathfinding and dendritic arborization can be manipulated by biochemical cues; however, neurite development can additionally be impacted by contacts with the local microenvironment. Herein, the impact of GMs with variable width and depth on hippocampal neurites was observed. Prior to plating and culture, hippocampal neurons were dissociated from glial cells, and glial cell growth was later inhibited to ensure the contact guidance applied to the neurites was dominated by the GMs and not the interaction between neurons and glial cells [19, 44]. Through four days in vitro, neurons successfully extended axons along the feature direction, regardless of the topography width, and formed expansive dendritic arborizations on flat controls (figures 4(b) and S5). Single topographies exhibit comparable axon and dendrite extension directionality [29]; however, few studies observe the impact on arborization expansion and axon growth preference [39]. Dendritic arborization exhibits significant reductions in coverage area in the presence of topographical features (figure 4(b)). Upon observation, the processes can climb in and out of grooves in all geometries [40, 48, 49]. The introduction of topographical cues likely induces a highly energy consumptive obstacle for the microtubules in the cytoarchitecture, which are inherently stiff, to overcome [40]. The lack of topography in controls allows more energy to be expended on lateral growth resulting in an expanded arborization. Continued culture until DIV 14 highlights the temporal consistency of these findings (not shown). GM depth imparts no significant change to arborization coverage area. Despite the ability to climb across shallow gratings, axons on 5 μ m wide gratings were predominantly guided in the direction of topographic cues, consistent with polarization

and elongation studies indicating plated neurons demonstrated increased axon presence on smaller topographies [33, 50]. Herein, we observed increased fluorescence of Tau-1 antibodies with decreasing topography width, particularly within the microgrooves (figure 5(g)). The relative orientation of the axon within the microgroove is also impacted by the width. Axons at DIV 4 extending on 80 μm show greater occurrence of growth along the interface of the ridge and groove in the topography. Elevated Tau-1 signal intensity migrated more centrally as the width decreased (figure 5(h)), suggesting 3D contact is vital to axonal differentiation from the original neurite. Taken together, increased axon presence and reduced dendritic arborization in smaller GM regions confirms the microtopographical substrate's impact on hippocampal neurite differentiation [51]. It should be noted however, reduced arborization could be greatly influenced by elevated soma density. Minimal differences in coverage area between ridge and groove adhered soma indicate a greater sensitivity to cell number over topographical geometries.

Primary hippocampal neurons successfully matured through DIV 14 on the GM surface and the impact on presynaptic structure and synaptogenesis was explored. Presynaptic structure was monitored via immunostaining of Synapsin 1, which has a specific role in synaptogenesis and often accumulates on synaptic vesicle membranes. Presynaptic assemblies have been observed at the neuron-substrate interface between neurons and both micro and nanostructures [52, 53]. Culture of hippocampal neurons on the GM did not result in elevated presynaptic puncta density relative to flat controls until the pattern width reached 5 μ m (figure 6(a)). This likely reflects the potential insensitivity of the puncta and neurites resulting from the larger length scales on the GM [39]. Synapsin 1 signal intensity has been shown to increase in the presence of submicron topography [54], indicating further decreasing the GM dimension will lead to an increase in presynapse formation. Significant increases in presynaptic density within the microgroove highlights the impact of topography induced increases in axon-dendrite interactions by upregulating axon growth (figure 5(g)). Further classification of neuron-neuron versus neuron-topography synapses is required to isolate and understand the direct influences of the microenvironment on the formation of presynaptic elements.

Synapsins play a crucial role in synapse formation and synaptic plasticity. Synapsin 1 has proven crucial for regulating release of neurotransmitter and is often associated with shortterm plasticity [55]. They achieve such function by stability modulation of synaptic vesicle reserve pools. Synaptic vesicle membranes are reversibly bound via activity-dependent phosphorylation [56–58]. When cultured along the GM, topographical stimuli induce reductions in Synapsin 1 signal intensity. Like puncta density, there was a general increase in signal intensity as the topography width decreased (figure 6(b)). Given synapsin's role in reserve pool stability, neurons cultured on large-scale topographies could induce neural networks more susceptible to impairment in the presence of prolonged action potentials. More mature presynaptic networks have been demonstrated on submicron fibrous scaffolds [54], therefore, the GM has induced an unstable and immature

network. One shortcoming of these studies is the lack of functional information. Future work is required to understand how physical topography impacts synaptic transmission between cells and how linear topographies impact the formation of excitatory or inhibitory synapses [24, 59, 60].

5. Conclusion

The GM developed herein applied mechanical stimuli via physical cues to primary hippocampal neurons, inducing morphological and synaptic network changes *in vitro*. The modular nature of the fabrication technique allows for manufacture of single substrates capable of supporting a variety of gradient dimensions in both width and depth. The GM was fabricated through clean room methods, which allow for high-throughput production. The GM represents a platform capable of supporting neuron cultures through development of a synaptic network, and further lends itself to more in depth and efficient understanding of the neuron-microenvironment interaction.

A neuron-on-chip platform exhibiting gradient, linear topographic features successfully supported primary hippocampal neurons through neural network formation. Neurons cultured on the PDMS GM demonstrated distinct influences on both morphologic and synaptic network parameters. The linear, ridge/groove topography was successfully modified with a surface enhancement protocol to increase neuron viability and acted as an adequate platform for neurons to mature through DIV 14. The average soma density per unit area was significantly increased relative to flat controls, allowing observation that neuronal adhesion was positively influenced by topographical stimuli. Analysis of neurite extension revealed a preferential growth environment for axons within the microgrooves of the GM and confirmed findings of microtopographies inhibiting the expansion of the dendritic arborization, limiting the formation of neuronal connectivity. Finally, a synaptic network was established, with reduced puncta density and synatptic protein signal intensity, indicating a potentially immature network. Depth modulation exhibited a more limited effect, reducing soma density in 20 μ m wide regions, increasing axon preference in 5 μ m microchannels, and inducing a sparser synaptic network. The overall effects of the GM on neuron behavior was thereby systematically understood by a one-step screening on an integrated chip, lending itself to improvements in neuroregenerative micro-device design.

Data availability statement

The data that support the findings of this study are available upon reasonable request from the authors.

Acknowledgments

This research was supported in part by the National Institutes of Health (Grant No. T32 EB006359 and R01 MH079407) and the National Science Foundation (Grant No. 1804787). We would like to thank Dr. Stephan Anderson and Dr. Xiaoguang

Zhao for their insightful guidance and providing technical support. We also want to thank Margaret O'Connor, Zachary Gardner, and Yuan Tian for their assistance in the preparation of primary neuron cultures.

ORCID iDs

Ryan McNaughton https://orcid.org/0000-0002-0584-4435

Xin Zhang https://orcid.org/0000-0002-4413-5084

References

- [1] Hasan M and Berdichevsky Y 2016 Neural circuits on a chip Micromachines 7 157
- [2] Li W, Xu Z, Huang J, Lin X, Luo R, Chen C-H and Shi P 2014 NeuroArray: a universal interface for patterning and interrogating neural circuitry with single cell resolution Sci. Rep. 4 4784
- [3] Peyrin J-M, Deleglise B, Saias L, Vignes M, Gougis P, Magnifico S, Betuing S, Pietri M, Caboche J and Vanhoutte P 2011 Axon diodes for the reconstruction of oriented neuronal networks in microfluidic chambers *Lab Chip* 11 3663–73
- [4] Renault R, Durand J-B, Viovy J-L and Villard C 2016 Asymmetric axonal edge guidance: a new paradigm for building oriented neuronal networks *Lab Chip* 16 2188–91
- [5] Hosmane S, Yang I H, Ruffin A, Thakor N and Venkatesan A 2010 Circular compartmentalized microfluidic platform: study of axon–glia interactions *Lab Chip* 10 741–7
- [6] Stenger D A, Hickman J J, Bateman K E, Ravenscroft M S, Ma W, Pancrazio J J, Shaffer K, Schaffner A E, Cribbs D H and Cotman C W 1998 Microlithographic determination of axonal/dendritic polarity in cultured hippocampal neurons J. Neurosci. Methods 82 167–73
- [7] Edwards D, Stancescu M, Molnar P and Hickman J J 2013 Two cell circuits of oriented adult hippocampal neurons on self-assembled monolayers for use in the study of neuronal communication in a defined system ACS Chem. Neurosci. 4 1174–82
- [8] Siddique R and Thakor N 2014 Investigation of nerve injury through microfluidic devices J. R. Soc. Interface 11 20130676
- [9] Kim H J, Park J W, Park J W, Byun J H, Vahidi B, Rhee S W and Jeon N L 2012 Integrated microfluidics platforms for investigating injury and regeneration of CNS axons *Ann. Biomed. Eng.* 40 1268–76
- [10] Shine H, Harcourt P and Sidman R 1985 Cultured peripheral nervous system cells support peripheral nerve regeneration through tubes in the absence of distal nerve stump *J. Neurosci. Res.* 14 393–401
- [11] Yu T T and Shoichet M S 2005 Guided cell adhesion and outgrowth in peptide-modified channels for neural tissue engineering *Biomaterials* 26 1507–14
- [12] Lacour S P, Atta R, FitzGerald J J, Blamire M, Tarte E and Fawcett J 2008 Polyimide micro-channel arrays for peripheral nerve regenerative implants *Sens. Actuators* A 147 456–63
- [13] Silver J and Miller J H 2004 Regeneration beyond the glial scar Nat. Rev. Neurosci. 5 146
- [14] Zhang Z, Rouabhia M, Wang Z, Roberge C, Shi G, Roche P, Li J and Dao L H 2007 Electrically conductive biodegradable polymer composite for nerve regeneration: electricity-stimulated neurite outgrowth and axon regeneration Artif. Organs 31 13–22

- [15] Tomba C, Braïni C, Wu B, Gov N S and Villard C 2014 Tuning the adhesive geometry of neurons: length and polarity control *Soft Matter* 10 2381–7
- [16] Taylor A M, Blurton-Jones M, Rhee S W, Cribbs D H, Cotman C W and Jeon N L 2005 A microfluidic culture platform for CNS axonal injury, regeneration and transport Nat. Methods 2 599
- [17] Dupin I, Dahan M and Studer V 2013 Investigating axonal guidance with microdevice-based approaches *J. Neurosci.* 33 17647–55
- [18] Bikbaev A, Frischknecht R and Heine M 2015 Brain extracellular matrix retains connectivity in neuronal networks Sci. Rep. 5 14527
- [19] Simitzi C, Ranella A and Stratakis E 2017 Controlling the morphology and outgrowth of nerve and neuroglial cells: the effect of surface topography *Acta Biomater.* 51 21–52
- [20] Farrukh A, Zhao S and Del Campo A 2018 Microenvironments designed to support growth and function of neuronal cells Front. Mater. 5 62
- [21] Tan K K, Tann J Y, Sathe S R, Goh S H, Ma D, Goh E L and Yim E K 2015 Enhanced differentiation of neural progenitor cells into neurons of the mesencephalic dopaminergic subtype on topographical patterns *Biomaterials* 43 32–43
- [22] Hanson Shepherd J N, Parker S T, Shepherd R F, Gillette M U, Lewis J A and Nuzzo R G 2011 3D microperiodic hydrogel scaffolds for robust neuronal cultures Adv. Funct. Mater. 21 47–54
- [23] Marcus M, Baranes K, Park M, Choi I S, Kang K and Shefi O 2017 Interactions of neurons with physical environments Adv. Healthcare Mater. 6 1700267
- [24] Czöndör K, Garcia M, Argento A, Constals A, Breillat C, Tessier B and Thoumine O 2013 Micropatterned substrates coated with neuronal adhesion molecules for high-content study of synapse formation *Nat. Commun.* 4 2252
- [25] Yoshida S, Kato-Negishi M and Takeuchi S 2018 Assembly and connection of micropatterned single neurons for neuronal network formation *Micromachines* 9 235
- [26] Piret G, Perez M-T and Prinz C N 2013 Neurite outgrowth and synaptophysin expression of postnatal CNS neurons on GaP nanowire arrays in long-term retinal cell culture *Biomaterials* 34 875–87
- [27] Yang K, Lee J, Lee J S, Kim D, Chang G-E, Seo J, Cheong E, Lee T and Cho S-W 2016 Graphene oxide hierarchical patterns for the derivation of electrophysiologically functional neuron-like cells from human neural stem cells ACS Appl. Mater. Interfaces 8 17763–74
- [28] Wu J, Mao Z, Tan H, Han L, Ren T and Gao C 2012 Gradient biomaterials and their influences on cell migration *Interface Focus* 2 337–55
- [29] Li W, Tang Q Y, Jadhav A D, Narang A, Qian W X, Shi P and Pang S W 2015 Large-scale topographical screen for investigation of physical neural-guidance cues Sci. Rep. 5 8644
- [30] Song R, Liang J, Lin L, Zhang Y, Yang Y and Lin C 2016 A facile construction of gradient micro-patterned OCP coatings on medical titanium for high throughput evaluation of biocompatibility J. Mater. Chem. B 4 4017–24
- [31] Park J, Kim D-H, Kim H-N, Wang C J, Kwak M K, Hur E, Suh K-Y, An S S and Levchenko A 2016 Directed migration of cancer cells guided by the graded texture of the underlying matrix *Nat. Mater.* 15 792
- [32] Kim D-H, Han K, Gupta K, Kwon K W, Suh K-Y and Levchenko A 2009 Mechanosensitivity of fibroblast cell shape and movement to anisotropic substratum topography gradients *Biomaterials* 30 5433–44
- [33] Micholt L, Gärtner A, Prodanov D, Braeken D, Dotti C G and Bartic C 2013 Substrate topography determines neuronal polarization and growth in vitro PLoS One 8 e66170

- [34] Lee S, Hong J and Lee J 2016 Cell motility regulation on a stepped micro pillar array device (SMPAD) with a discrete stiffness gradient *Soft Matter* 12 2325–33
- [35] Fricke R, Zentis P D, Rajappa L T, Hofmann B, Banzet M, Offenhäusser A and Meffert S H 2011 Axon guidance of rat cortical neurons by microcontact printed gradients *Biomaterials* 32 2070–6
- [36] Stanganello E, Zahavi E E, Burute M, Smits J, Jordens I, Maurice M M, Kapitein L C and Hoogenraad C C 2019 Wnt signaling directs neuronal polarity and axonal growth iScience 13 318–27
- [37] Chung B G, Flanagan L A, Rhee S W, Schwartz P H, Lee A P, Monuki E S and Jeon N L 2005 Human neural stem cell growth and differentiation in a gradient-generating microfluidic device *Lab Chip* 5 401–6
- [38] Li G, Chen S, Zeng M, Kong Y, Zhao F, Zhang L and Yang Y 2019 Hierarchically aligned gradient collagen micropatterns for rapidly screening Schwann cells behavior *Colloids Surf.* B 176 341–51
- [39] McNaughton R C, Huo Y, Li G, Zhao X, Man H and Zhang X 2019 Comprehensive, high throughput screening of neuron behavior on gradient micro-alignment topographies 2019 20th Int. Conf. on Solid-State Sensors, Actuators and Microsystems & EUROSENSORS XXXIII (TRANSDUCERS & EUROSENSORS XXXIII) (IEEE) pp 1078–81
- [40] Chua J S, Chng C-P, Moe A A K, Tann J Y, Goh E L, Chiam K-H and Yim E K 2014 Extending neurites sense the depth of the underlying topography during neuronal differentiation and contact guidance *Biomaterials* 35 7750–61
- [41] Mahoney M J, Chen R R, Tan J and Saltzman W M 2005 The influence of microchannels on neurite growth and architecture *Biomaterials* 26 771–8
- [42] Burbulla L F, Beaumont K G, Mrksich M and Krainc D 2016 Micropatterning facilitates the long-term growth and analysis of iPSC-derived individual human neurons and neuronal networks Adv. Healthcare Mater. 5 1894–903
- [43] Nicholls J G, Martin A R, Wallace B G and Fuchs P A 2001 From Neuron to Brain vol 271 (Sunderland, MA: Sinauer Associates)
- [44] Kitazawa A, KI K, Hayashi K, Matsunaga Y, Ishii K and Nakajima K 2014 Hippocampal pyramidal neurons switch from a multipolar migration mode to a novel "climbing" migration mode during development *J. Neurosci*. 34 1115–26
- [45] Revell S M H 2011 Symptom clusters in traumatic spinal cord injury: an exploratory literature review J. Neurosci. Nurs. 43 85–93
- [46] Smith L and Ma P 2004 Nano-fibrous scaffolds for tissue engineering Colloids Surf. B 39 125–31
- [47] Roach P, Parker T, Gadegaard N and Alexander M R 2013 A bio-inspired neural environment to control neurons comprising radial glia, substrate chemistry and topography *Biomater. Sci.* 1 83–93
- [48] Hoffman-Kim D, Mitchel J A and Bellamkonda R V 2010 Topography, cell response, and nerve regeneration *Annu. Rev. Biomed. Eng.* 12 203–31
- [49] Li N and Folch A 2005 Integration of topographical and biochemical cues by axons during growth on microfabricated 3D substrates Exp. Cell Res. 311 307–16
- [50] Kam L, Shain W, Turner J and Bizios R 2001 Axonal outgrowth of hippocampal neurons on micro-scale networks of polylysine-conjugated laminin *Biomaterials* 22 1049–54
- [51] Greene A C, Washburn C M, Bachand G D and James C D 2011 Combined chemical and topographical guidance cues for directing cytoarchitectural polarization in primary neurons *Biomaterials* 32 8860–9

- [52] Lucido A L, Sanchez F S, Thostrup P, Kwiatkowski A V, Leal-Ortiz S, Gopalakrishnan G, Liazoghli D, Belkaid W, Lennox R B and Grutter P 2009 Rapid assembly of functional presynaptic boutons triggered by adhesive contacts *J. Neurosci.* 29 12449–66
- [53] Anava S, Greenbaum A, Jacob E B, Hanein Y and Ayali A 2009 The regulative role of neurite mechanical tension in network development *Biophys. J.* 96 1661–70
- [54] Yin Y, Huang P, Han Z, Wei G, Zhou C, Wen J, Su B, Wang X and Wang Y 2014 Collagen nanofibers facilitated presynaptic maturation in differentiated neurons from spinal-cord-derived neural stem cells through MAPK/ERK1/2-synapsin I signaling pathway Biomacromolecules 15 2449–60
- [55] Fornasiero E F, Bonanomi D, Benfenati F and Valtorta F 2010 The role of synapsins in neuronal development *Cell. Mol. Life Sci.* 67 1383–96

- [56] Chi P, Greengard P and Ryan T A 2001 Synapsin dispersion and reclustering during synaptic activity *Nat. Neurosci.* 4 1187–93
- [57] Hilfiker S, Pieribone V A, Czernik A J, Kao H-T, Augustine G J and Greengard P 1999 Synapsins as regulators of neurotransmitter release *Phil. Trans. R. Soc.* B 354 269–79
- [58] Cesca F, Baldelli P, Valtorta F and Benfenati F 2010 The synapsins: key actors of synapse function and plasticity *Prog. Neurobiol.* 91 313–48
- [59] Jakobsson A, Ottosson M, Zalis M C, O'Carroll D, Johansson U E and Johansson F 2017 Three-dimensional functional human neuronal networks in uncompressed low-density electrospun fiber scaffolds *Nanomedicine* 13 1563–73
- [60] Zhang J, Venkataramani S, Xu H, Song Y-K, Song H-K, Palmore G T R, Fallon J and Nurmikko A V 2006 Combined topographical and chemical micropatterns for templating neuronal networks *Biomaterials* 27 5734–9